DETERMINATION OF IN-FLIGHT AVIRIS SPECTRAL, RADIOMETRIC, SPATIAL AND SIGNAL-TO-NOISE CHARACTERISTICS USING ATMOSPHERIC AND SURFACE MEASUREMENTS FROM THE VICINITY OF THE RARE-EARTH-BEARING CARBONATITE AT MOUNTAIN PASS, CALIFORNIA

ROBERT O. GREEN, GREGG VANE and JAMES E. CONEL, Jet Propulsion Laboratory, 4800 Oak Grove Drive, Pasadena, CA 91109

ABSTRACT

An assessment of the Airborne Visible/Infrared Imaging Spectrometer (AVIRIS) performance was made for a flight over Mountain Pass, California, July 30, 1987. The flight data were reduced to reflectance using an empirical algorithm which compensates for solar, atmospheric and instrument factors. AVIRIS data in conjunction with surface and atmospheric measurements acquired concurrently were used to develop an improved spectral calibration. We also performed an accurate in-flight radiometric calibration using the LOWTRAN 7 radiative transfer code together with measured surface reflectance and atmospheric optical depths. A direct comparison with coincident Thematic Mapper imagery of Mountain Pass was used to demonstrate the high spatial resolution and good geometric performance of AVIRIS. The in-flight instrument noise was independently determined with two methods which showed good agreement. A signal-to-noise ratio was calculated using data from a uniform playa. This ratio was scaled to the AVIRIS reference radiance model, which provided a basis for comparison with laboratory and other in-flight signal-to-noise determinations.

1.0 INTRODUCTION

The performance characteristics of AVIRIS in the laboratory environment have been measured through a series of calibrations over the past year of instrument development (Vane et al., 1987, 1988). The objectives of this experiment were to develop and apply methods for assessing the in-flight spectral, radiometric, spatial and signal-to-noise performance of the instrument and to provide an in-flight spectral and radiometric calibration.

AVIRIS data were acquired over the Mountain Pass region on the 30th of July, 1987, 10:15 AM PST, under clear sky conditions. Concurrent surface reflectance measurements were collected at the playa, asphalt and graded soil targets. These areas were selected for surface homogeneity, for contrast in albedo and for aerial extent significantly greater than an AVIRIS resolution element. A spectrum of the mineral bastnaesite, which occurs at Mountain Pass (Olson et al., 1954) was independently measured with a laboratory spectrometer. Bastnaesite contains narrow spectral absorption features in the visible and near infrared which are suitable for assessing AVIRIS spectral performance. Atmospheric optical depth measurements were acquired contemporaneously with the over-flight. The coverage of the flight data and the location of the surface targets are shown in Figure 1. Thematic Mapper (TM) satellite data were obtained with coverage encompassing the Mountain Pass experiment region.
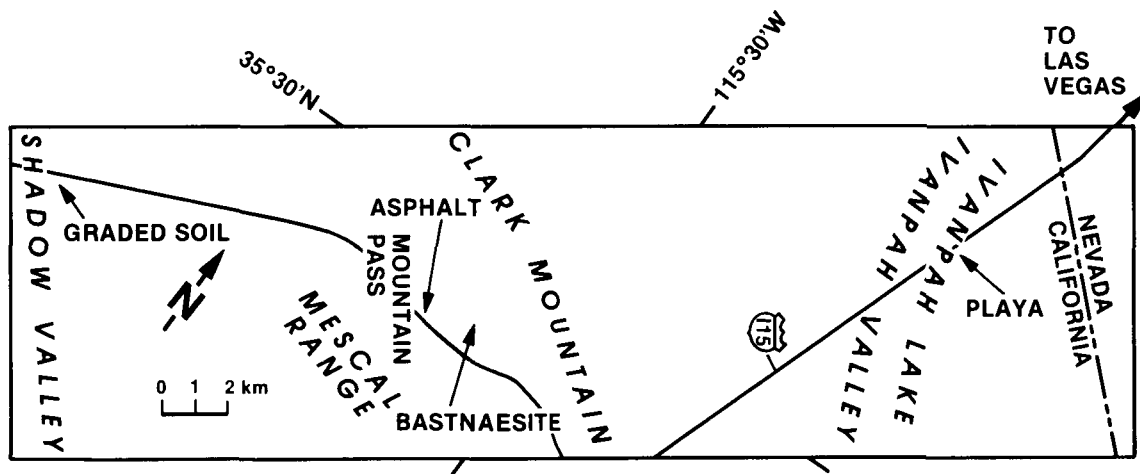

Figure 1. Location of AVIRIS flight data over the Clark Mountains on July 30th, 1987 at 10:15 AM PST. The positions of the playa, bastnaesite, asphalt and graded soil target areas are indicated.

With these data the in-flight performance of AVIRIS was determined. Additionally, a spectral and radiometrical calibration was generated for these imaging spectrometer data. We describe in the paper the data used, the methods of analysis, and results obtained.

2.0 DATA USED IN THE STUDY

2.1 AVIRIS Image Data.

AVIRIS data of 2048 image lines by 614 cross-track samples and 224 spectral channels were acquired on an east to west flight line from the Ivanpah Playa across Clark Mountain to Shadow Valley. The data were corrected through subtraction of the end-of-line dark current and spatial resampling to correct for detector readout delay (Vane et al, 1987). These corrections generated data that were proportional to total radiance and spatially registered between spectral channels. Corrected AVIRIS spectra from the playa, the bastnaesite locality, the asphalt and the graded soil targets are plotted in Figure 2. The playa data were taken from a 200 by 200 meter homogeneous area of Ivanpah Playa and represent an average of 100 AVIRIS spatial elements. The bastnaesite spectrum was extracted from 4 contiguous resolution elements. The asphalt target is a large recently surfaced parking lot from which 12 spatial elements were extracted and averaged. The soil target was derived from an average of 12 resolution elements selected from a large area of recently graded soil.
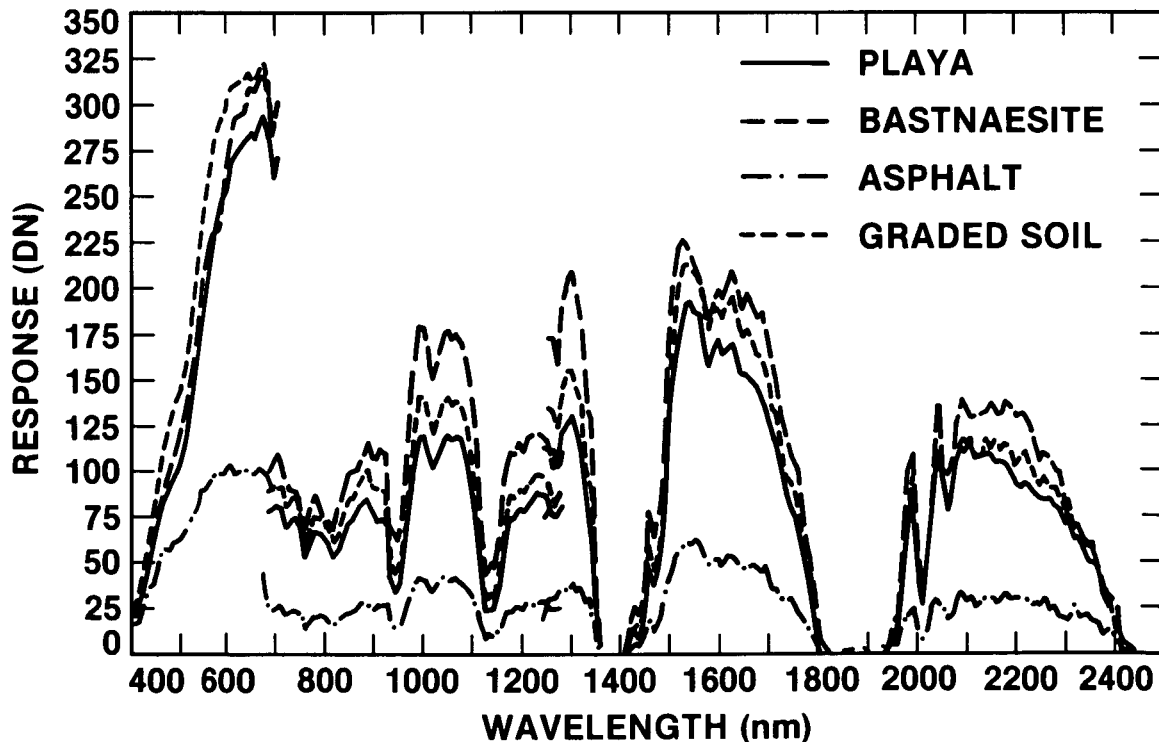

Figure 2. AVIRIS spectra of the playa, bastnaesite, asphalt and graded soil targets with compensated dark current and detector readout delay. These data represent averages of 100, 4, 12 and 12 pixels respectively.

2.2 Surface Reflectance Data.

The Portable Instantaneous Display and Analysis Spectrometer (PIDAS) (Goetz, 1987) was used to acquire in situ surface reflectance spectra for the playa, asphalt and graded soil targets. The eight second spectral acquisition time of the instrument allowed the collection of 102, 93 and 35 spectra for the playa, asphalt and soil targets respectively in the period between 10:00 AM and noon. These data have a spectral sampling interval of better than 5 nm in the wavelength region from 450 to 2450 nm, and were reduced to reflectance using spectra of a pressed halon reference target. For comparisons and calculations using these reflectance spectra and the AVIRIS data, the PIDAS spectra were convolved with the AVIRIS channel response functions. The resulting reflectance spectra, reduced to AVIRIS spectral resolution, are plotted in Figure 3. Standard deviations of 1, 1 and 2 percent reflectance were calculated for the playa, asphalt and soil respectively, confirming the nearly homogeneous surface reflectance of these targets. A
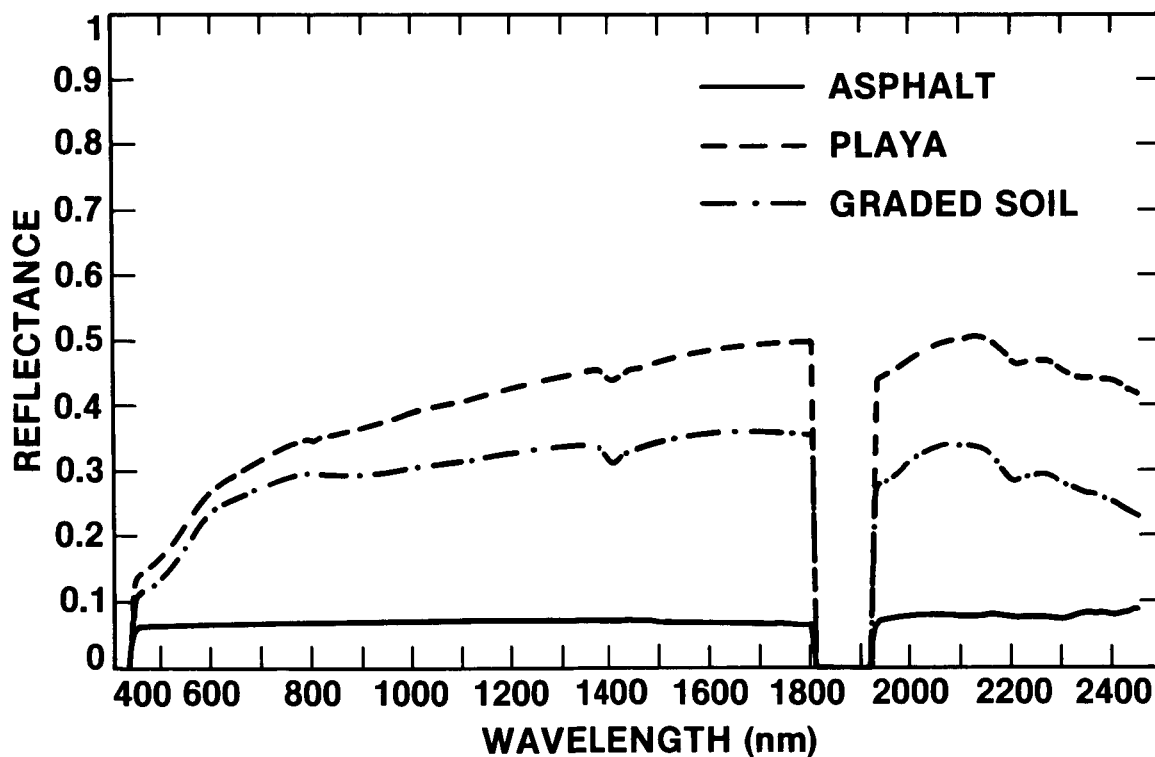

Figure 3. PIDAS reflectance spectra of the asphalt, playa and graded soil target acquired contemporaneously with the AVIRIS flight data. The data are averages of 102, 93 and 35 spectra and have been convolved with the AVIRIS channel spectral response functions.

laboratory reflectance spectrum of the mineral bastnaesite, acquired independently with a Beckman UV5240 spectrometer, is plotted in Figure 4.
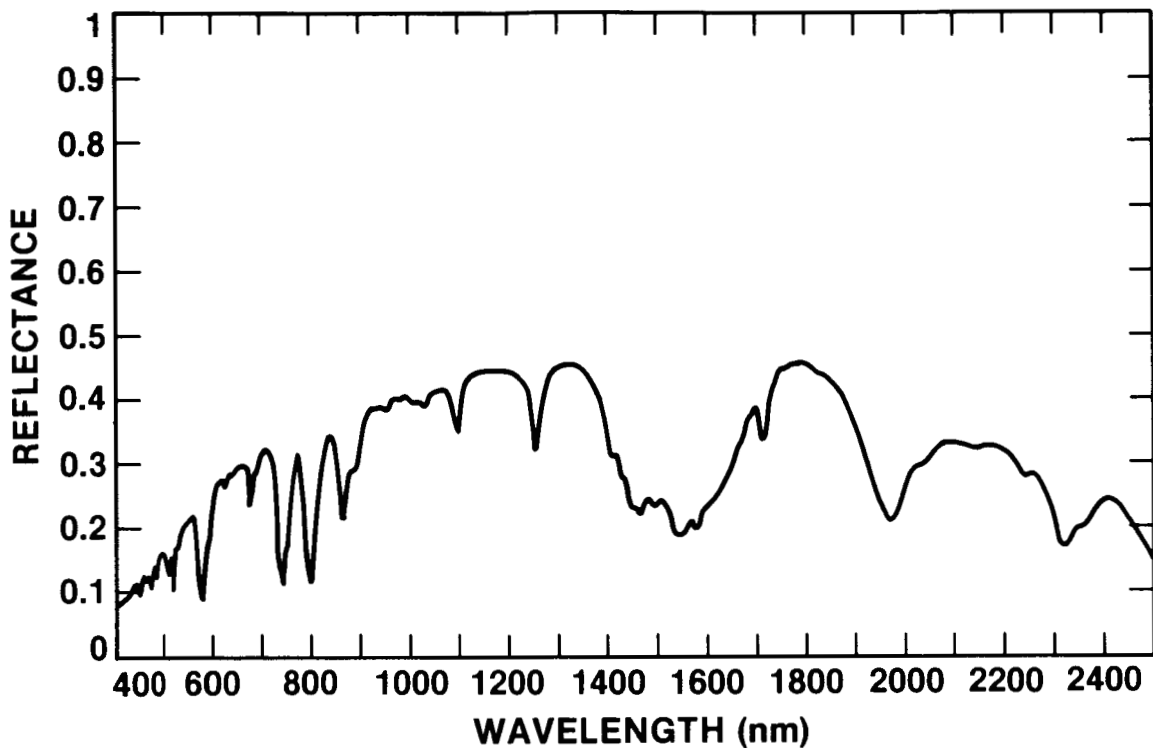

Figure 4. A reflectance spectrum of the mineral bastnaesite acquired with a Beckman UV5240 laboratory spectroradiometer showing the narrow absorption features in the visible and near infrared region of the spectrum caused by trivalent rare earth elements (Adams, 1965)

2.3 Atmospheric Measurements.

Solar illumination measurements were acquired with a Reagan-type radiometer (Shaw et al, 1973) from 7:32 am to 11:55 am at ten minute intervals from an elevated site at the asphalt target on the day of the overflight. Atmospheric optical depths were determined from standard Langley plots, as described in Herman et al, (1978). The optical depths for the ten wavelength positions with 10 nm filter bandwidths are given in Table 1.

Table 1. Optical depth measurements at Mountain Pass, CA.

Center Wavelength (nm)	Calculated Optical Depth
370	0.551
400	0.417
440	0.305
520	0.197
610	0.154
670	0.105
780	0.069
870	0.056
940	0.398
1003	0.047

3.0 DATA REDUCTION

3.1 Empirical Line Reflectance Recovery.

The empirical line algorithm, described for example in Conel et al, (1987), recovers surface reflectance from instrument response data. The method compensates for multiplicative components of solar illumination, atmospheric attenuation and instrument response. Additionally, the additive factors of atmospheric path radiance and instrument dark current are removed.

The algorithm requires two targets of contrasting albedo and equivalent spectral resolution for which both surface reflectance and AVIRIS instrument response are known. Two first order linear equations are developed of the form

$$DN = A * R + B$$

where DN is the instrument response, R is the surface reflectance, A accounts for the solar, atmospheric and instrument multiplicative factors and B for the instrument and atmospheric additive components. These equations are solved for A and B for each AVIRIS spectral channel. The resulting equation

$$R = (DN - B) / A$$

is formed with the determined multiplicative and additive factors, which transform instrument DN to reflectance for the entire imaging

spectrometer data set. Primary assumptions of the algorithm are a constant instrument performance and a uniform atmosphere over the region to which it is applied.

The algorithm was implemented with the reflectance spectra measured with PIDAS at the asphalt and graded soil targets and the corresponding instrument response (Figures 2 and 3). An empirical line spectrum derived from AVIRIS data over the bastnaesite target after the application of the algorithm resolves the narrow neodynium absorption features between 700 and 940 nm (Figure 5).
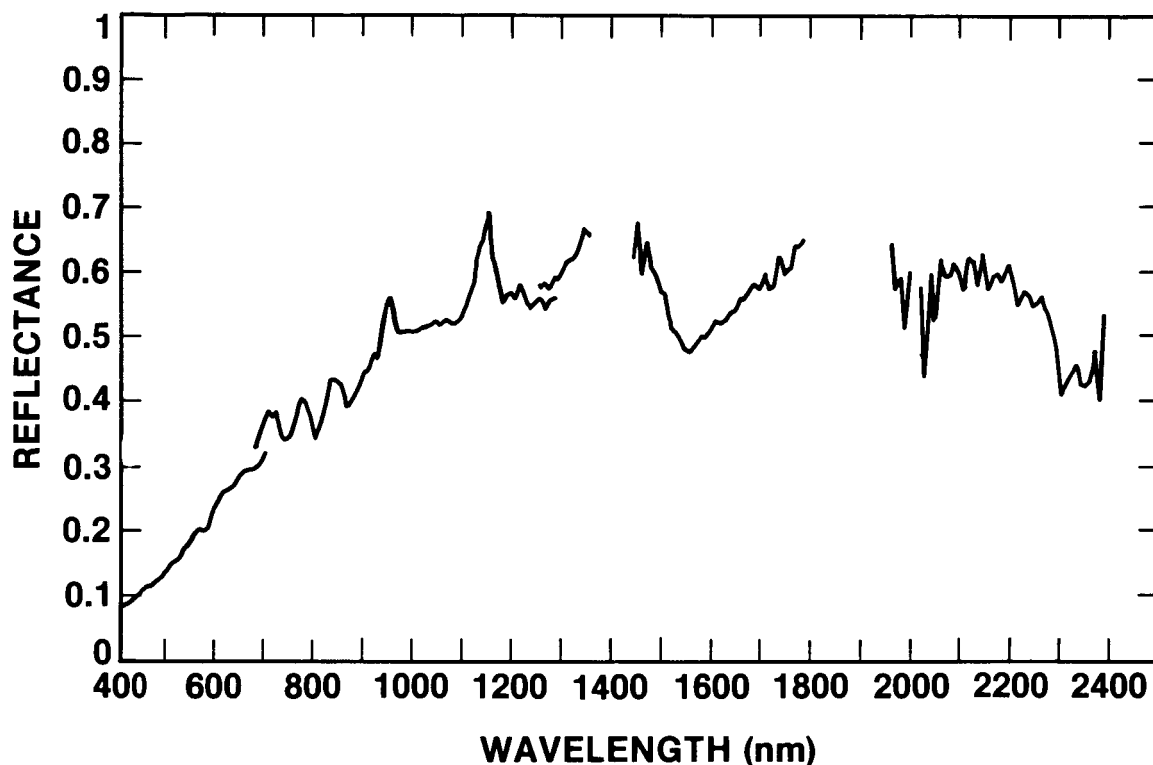

Figure 5. Spectra derived from AVIRIS data using the empirical line reflectance retrieval algorithm. The three strong neodynium absorption features between 700 and 900 nm are well resolved. Other features in the spectrum are discussed in the text.

The anomalous reflectance peaks at 940 and 1125 nm are due to the difference in atmospheric water vapor content between the bastnaesite and empirical line targets. This demonstrates that the assumption of uniform atmosphere is not true in regions of atmospheric water absorption. We (Conel, et al, 1988a) have subsequently mapped the variations in atmospheric water vapor with elevation using the AVIRIS channel responses in the 940 and 1125 nm water bands. The offsets in the reflectance curves at approximately 700 and 1280 nm are due to changes in the response functions of spectrometers A and B over the course of the flight line (Vane et al., 1988). The gaps at about 1400 and 1900 nm are due to

the strong atmospheric water bands, and the gap at about 2000 nm is due to a noisy detector element in spectrometer D. These features can be seen in most of the full spectrum plots in this paper.

3.2 LOWTRAN 7 Radiance Model.

In situ measurements of surface reflectance and atmospheric optical depth were used in conjunction with the radiative transfer code LOWTRAN 7 (Kneizys et al, 1988) to calculate the total radiance at AVIRIS for the Mountain Pass overflight. The atmospheric path and surface reflected as well as the total radiance for the Ivanpah Playa target are plotted in Figure 6. An extensive discussion of this methodology for modeling radiance with radiative transfer codes and surface and atmospheric measurements is given in Conel et al, (1988b). The high resolution atmospheric gas absorptions provide features suitable for assessment of the in-flight spectral performance, while modeled total radiance allows evaluation of the radiometric calibration.
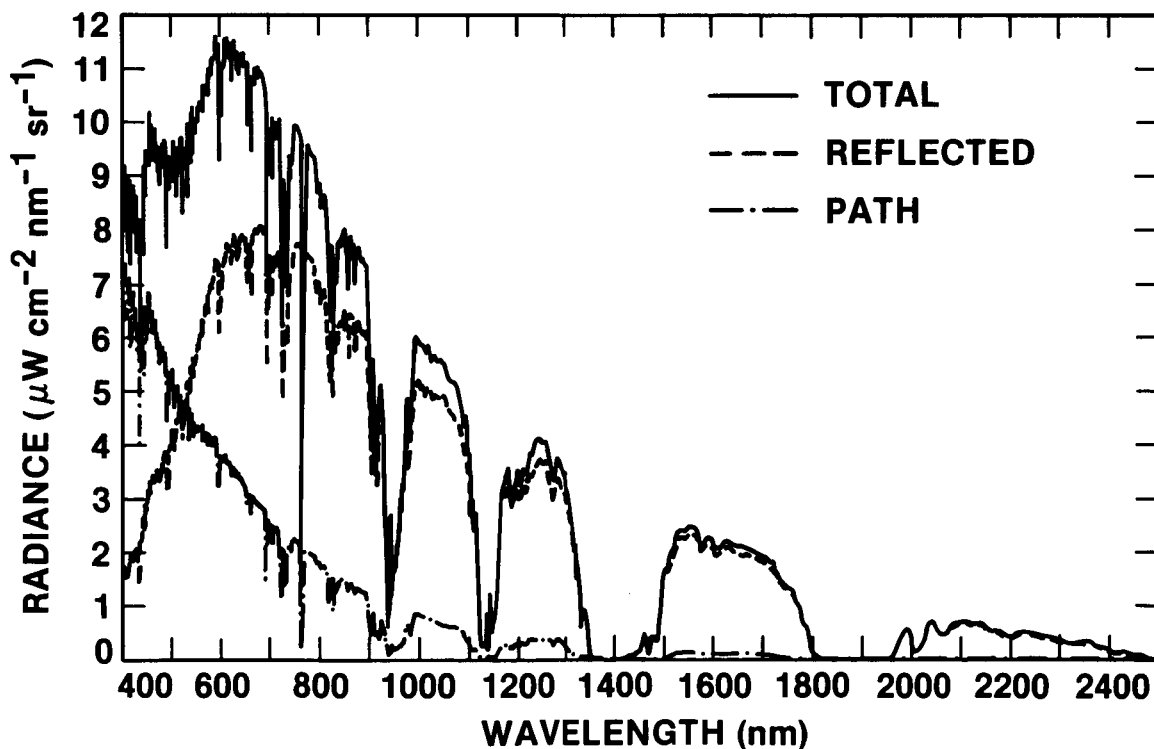

Figure 6. A LOWTRAN 7 model radiance for Ivanpah Playa constrained by the conditions of the AVIRIS overflight. The atmospheric path, surface reflected and total radiances are plotted. The path radiance is a significant contributor, ranging from 80 to 10 percent of the total from 400 to 1300 nm.

4.0 ANALYSES AND RESULTS

4.1 Spectral Performance and calibration.

In-flight spectral performance was assessed using the neodymium absorption features between 700 and 940 nm and various atmospheric gaseous absorption features that occur throughout the spectral region of AVIRIS.

To provide a common basis for comparison the laboratory bastnaesite spectrum was convolved with the preflight season channel wavelength positions and spectral response functions. Figure 7 shows the Gaussian approximation for the spectral response function for AVIRIS channel 98 with the wavelength position determined as the wavelength of maximum amplitude and spectral response characterized as the full width at half maximum amplitude (FWHM). The correspondence of AVIRIS spectral response to a Gaussian function is consistent with the instrument design and
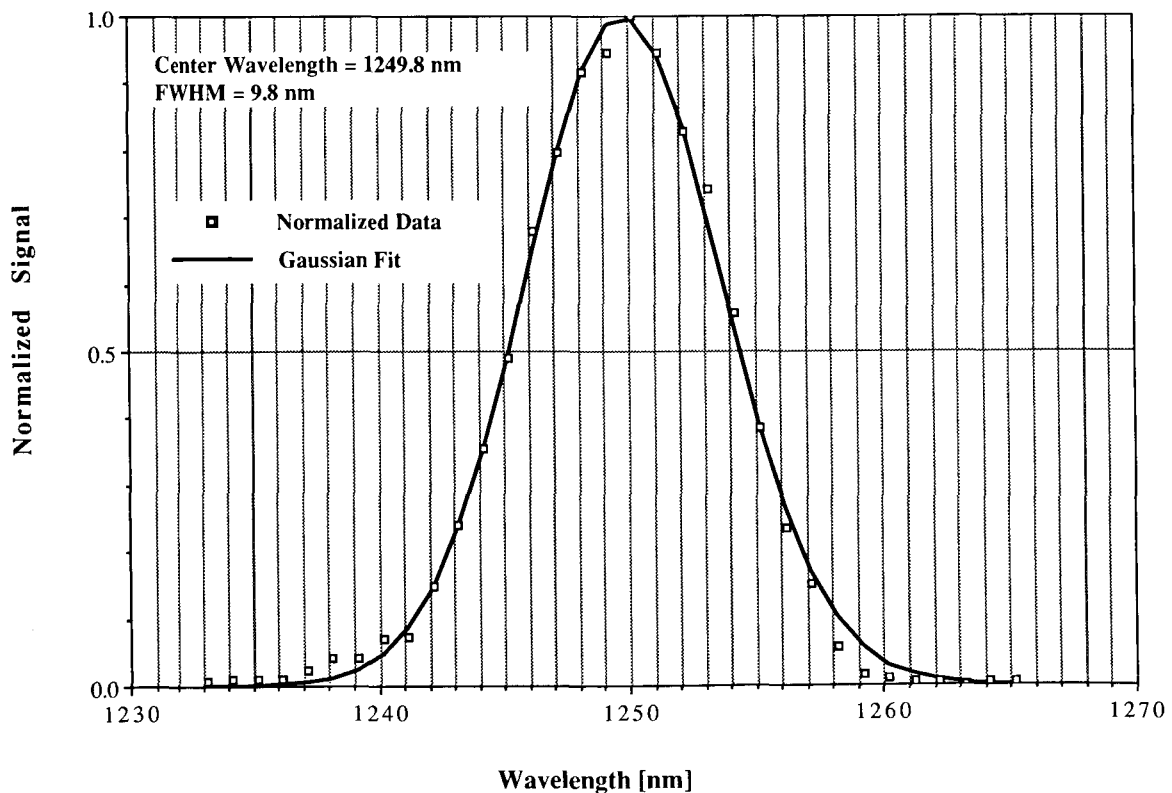

Figure 7. A typical normalized AVIRIS spectral response function for channel 98, spectrometer C, compared to a Gaussian representation which closely approximates the measured function.

laboratory determination (Macenka and Chrisp 1987, and Vane et al, 1988). In Table 2 the pre-season spectral calibration is presented (Vane et al, 1987) such that the spectral position of an AVIRIS detector is determined by the product of the detector number and the sampling interval summed with the starting wavelength position of the spectrometer. Both the convolved laboratory measured bastnaesite spectrum and the AVIRIS empirical line spectrum are plotted in Figure 8 for the wavelength region between 700 and 940 nm. A spectral shift of several nanometers of the AVIRIS spectrum

Table 2. Pre-season laboratory spectral calibration

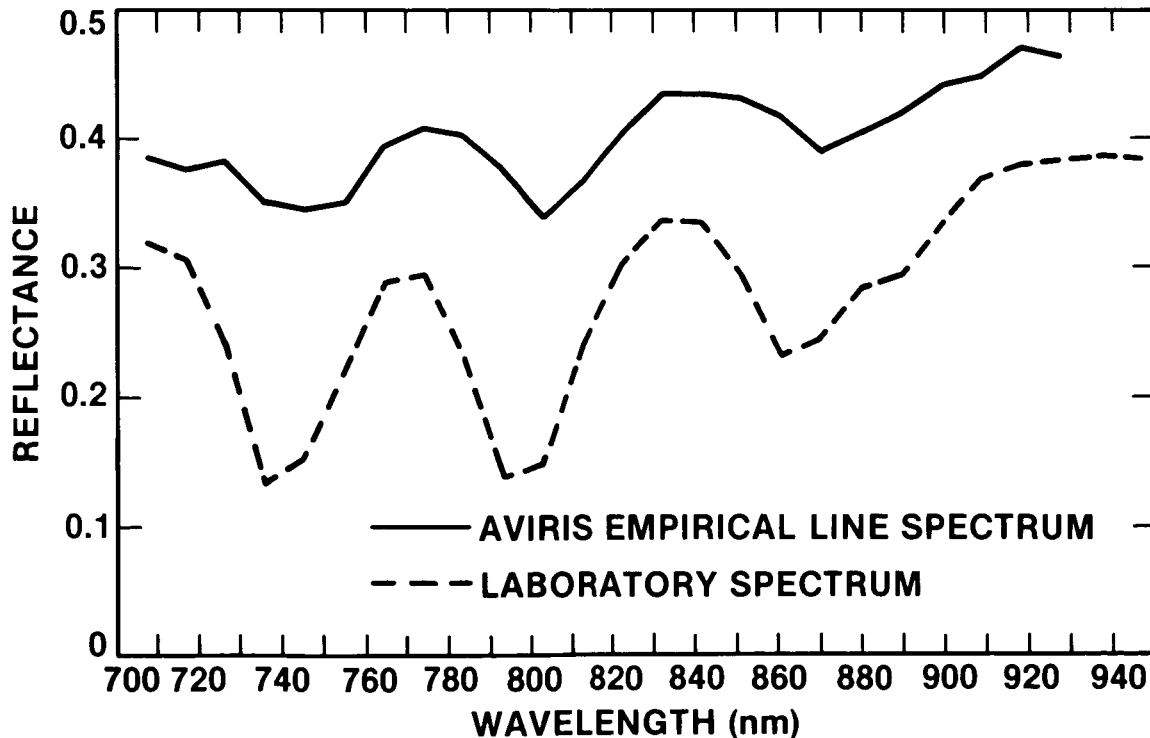| Spectrometer	Sampling Int. (nm)	Starting Pos. (nm)	Detector Number	Response Width (nm)
A	9.858	396.5	0 - 31	9.7
B	9.579	678.2	0 - 63	9.7
C	9.849	1241.7	0 - 63	9.0
D	9.859	1828.8	0 - 63	11.6

Figure 8. An empirical line derived bastnaesite spectrum compared to a Beckman spectrum of bastnaesite showing a shift of AVIRIS in-flight spectral position to shorter wavelengths.

to longer wavelengths is observed. This indicates the spectral channel positions for spectrometer B are shifted to shorter wavelengths for these flight data as compared to the laboratory measured bastnaesite spectrum.

To utilize the atmospheric absorption features in an independent assessment of in-flight spectral performance, the LOWTRAN 7 total radiance was convolved with the preflight season AVIRIS channel spectral positions and response functions and compared with the AVIRIS in-flight radiance over Ivanpah Playa. Figure 9 shows the results for each of the four AVIRIS spectrometers. Spectrometer B exhibits a shift in spectral alignment to longer wavelengths, which is consistent with the determination derived from the bastnaesite spectrum. Spectrometer D likewise shows a shift to shorter wavelengths, while spectrometers A and C show good agreement between in-flight and laboratory spectral alignment. The predicted total radiance at AVIRIS allows evaluation of the in-flight spectral response. For
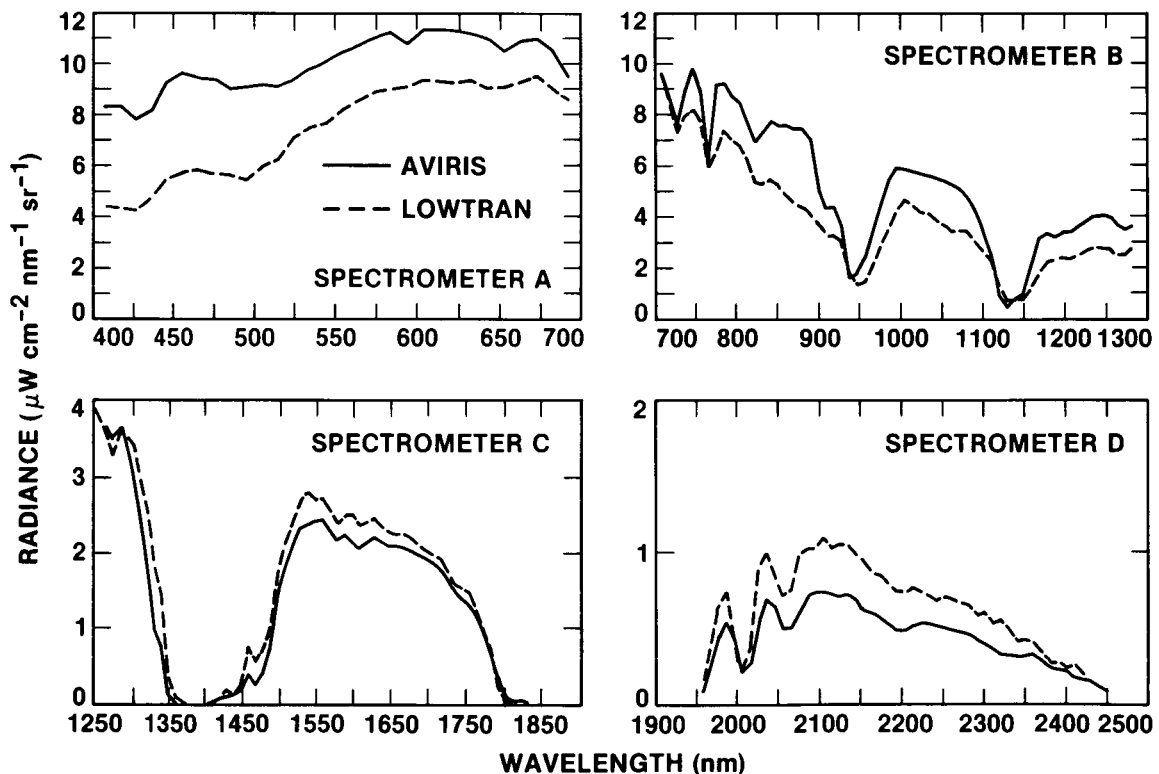

Figure 9. A comparison of AVIRIS radiance to LOWTRAN 7 modeled radiance for spectrometers A through D. Spectrometer B exhibits a broadened spectral response function and a shift to shorter wavelengths relative to the predicted LOWTRAN 7. Spectrometer D has also shifted several nanometers to shorter wavelengths, while spectrometers A and C show good agreement with the LOWTRAN 7 model.

spectrometer B , the atmospheric oxygen feature at 760 nm is more completely resolved in the LOWTRAN 7 modeled data than the in-flight data indicating a broadening of spectral response at the time of flight data acquisition. This broadening of the spectral response function is evident in the water bands at 735, 840, 940 and 1125 nm as well.

Using the LOWTRAN 7 model, an algorithm was developed to optimize for the Gaussian function which best describes the in-flight AVIRIS channel wavelength position and spectral response function. This algorithm minimizes the mean squared radiance difference between the AVIRIS retrieved radiance and modeled radiance while varying the response width and position of the Gaussian function convolved with the LOWTRAN 7 model. The algorithm was applied to sharp atmospheric absorption features where a change in position and response strongly affects the returned radiance. The spectral characteristics for spectrometer A were determined using the the water absorption band near 675 nm. The absorptions between 700 and 850 nm were used to fit the spectral characteristics for spectrometer B, while the carbon dioxide doublets centered at 1600 and 2050 nm were used for spectrometers C and D respectively. An example of the results for this minimizing algorithm for spectrometer C is given in Figure 10a and b. The spectral position is optimized for 1 nm to shorter wavelengths than the pre-season calibration (Figure 10a), while the spectral response is characterized by 1 nm less than the nominal 10 nm FWHM response function (Figure 10b). Table 3 describes the resulting in-flight spectral calibration derived using this error
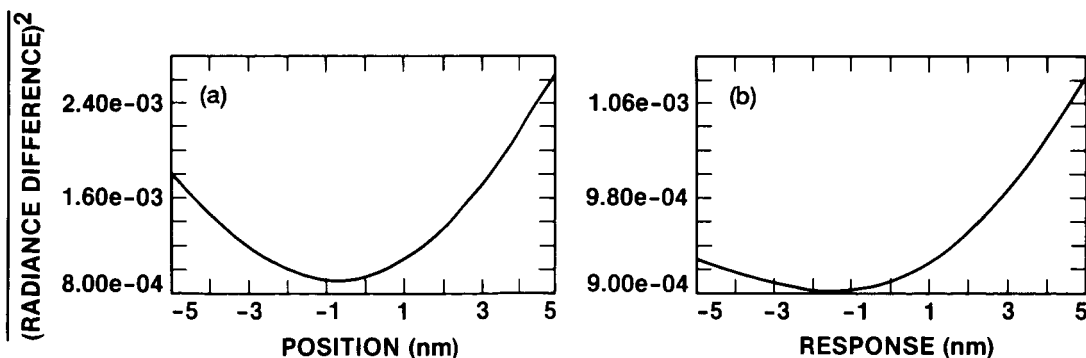

Figure 10. (a) Least squared residual fit for AVIRIS in-flight spectral position as a function of deviation from the pre-flight season laboratory calibration. The wavelength position for spectrometer C is optimized with a 1 nm shift to shorter wavelengths. (b) Residual minimization for spectral response function as deviation from a 10 nm Gaussian. Spectral response is optimal for a full width at half maximum of 9 nm.

minimization algorithm for each of the spectrometers. The plots in Figure 11 show the result of application of the in-flight spectral calibration to the AVIRIS flight data in comparison with the radiance curves obtained from LOWTRAN 7. Compared with Figure 9, an improvement can been seen in terms both of correspondence of wavelength position and resolution of the atmospheric absorption features.

TABLE 3. In-flight spectral calibration.

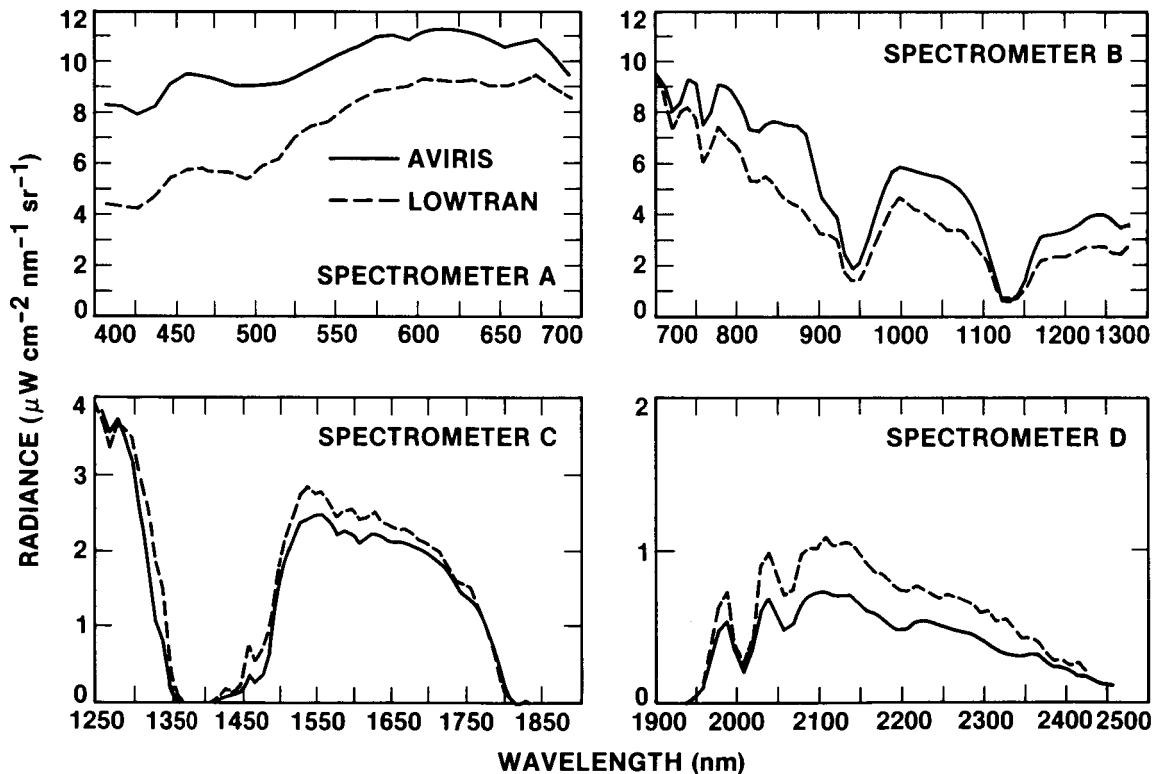| Spectrometer	Sampling Int. (nm)	Starting Pos. (nm)	Detector Number	Response Width (nm)
A	9.858	396.5	0 - 31	15
B	9.579	674.2	0 - 63	17
C	9.849	1240.7	0 - 63	9
D	9.859	1831.8	0 - 63	10

Figure 11. Results of the application of the in-flight determined spectral calibration. The spectral positions of spectrometers B and C are significantly improved as is the spectral resolution of spectrometer B.

4.2 Radiometric Performance and calibration.

In Figure 9 some level of disagreement in all four spectrometers between the AVIRIS laboratory calibrated total radiance and the LOWTRAN 7 modeled radiance over Ivanpah Playa is observed. A ratio of these data in Figure 12 shows the LOWTRAN 7 modeled radiance is on the average 1.2 times that of AVIRIS in spectrometer A, 1.4 in B, 0.85 in C and 0.80 in D. The various factors contributing to these discrepancies are discussed by Vane et al. (1988).
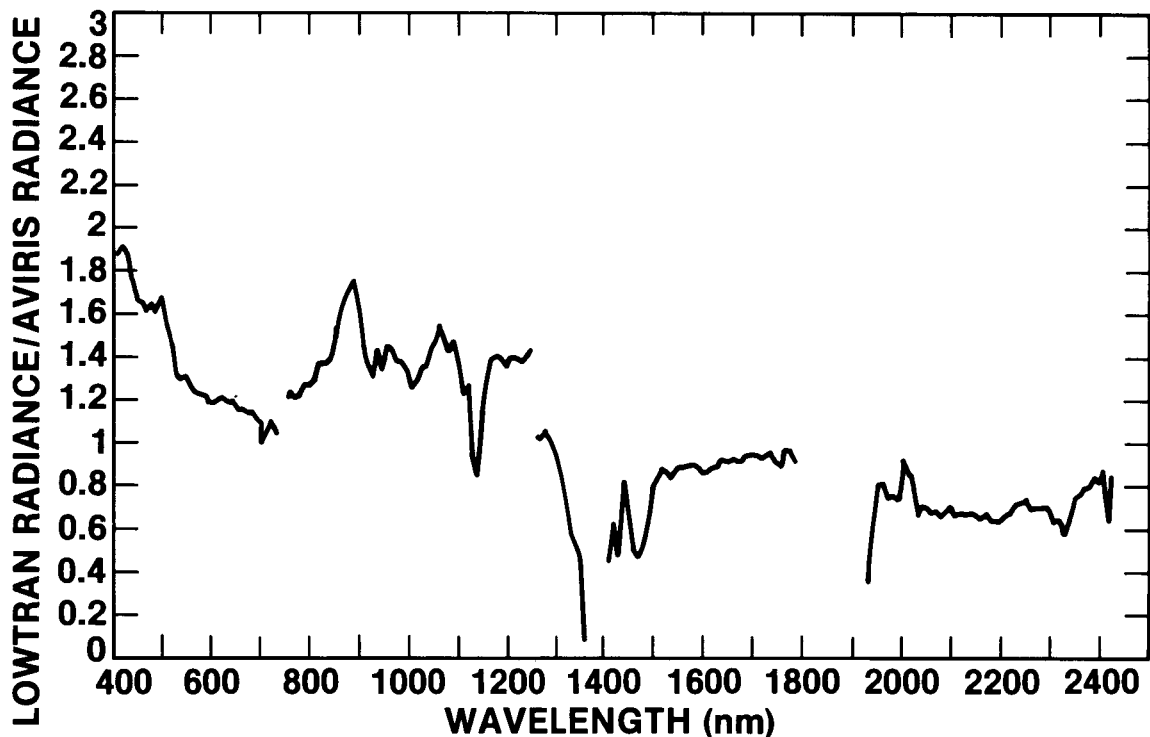

Figure 12. Ratio of LOWTRAN 7 modeled radiance to radiance derived by applying the pre-flight season radiometric calibration to AVIRIS data from Ivanpah Playa. The deviation from a ratio of 1 indicates the amount of disagreement between the laboratory and in-flight radiometric response function of AVIRIS.

Using the LOWTRAN 7 radiance model, an improved in-flight radiometric calibration was achieved by constructing the ratio of LOWTRAN 7 total radiance to AVIRIS in-flight instrument response. These factors for the in-flight radiometric calibration of the Mountain Pass data set, which transform instrument response into radiance, are plotted in Figure 13. This calibration provides a basis for analysis of these AVIRIS data requiring accurate units of total radiance.
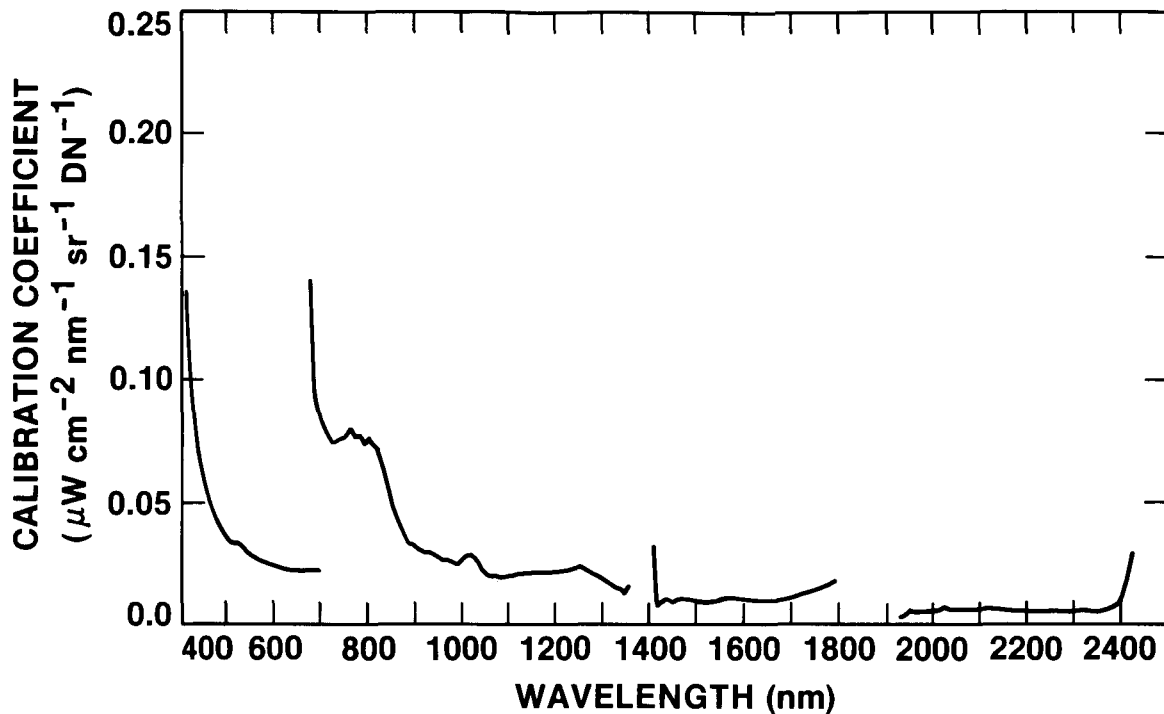
Figure 13. Radiometric calibration factors determined for the Mountain Pass flight data. The coefficients provide an accurate transformation of AVIRIS instrument response in DN to total radiance incident at the instrument.

4.3 Spatial Performance

As a preliminary evaluation of spatial resolution and intra-image geometric quality, images of the AVIRIS and TM data were compared over the Mountain Pass site as shown in Figure 14 (slide No. 12). The AVIRIS 10-nm channels were averaged to correspond to the broad TM channels centered at 660, 1650 and 2200 nm; the data are displayed as red, green and blue respectively. The spatially varying geological and cultural surface features provide a basis for comparison of spatial resolution. AVIRIS resolves the two strands of Interstate 15 and the detailed geological stratigraphy to the south of the road which are not as clearly discernable in the TM image. This observed higher spatial resolution of AVIRIS is consistent with the designed 20 m ground instantaneous field of view (GIFOV) and 17 m pixel-to-pixel spacing of AVIRIS, compared to the 30 m GIFOV and 28.5 m pixel-to-pixel spacing of TM. The intra-image geometric fidelity of the AVIRIS and TM images is comparable. The AVIRIS image has had no geometric correction applied to it other than the limited on-board roll correction which is applied in flight (Porter and Enmark, 1987).

THEMATIC MAPPER

AVIRIS

N

SCENE 850043 7424
PATH 39
ROW 35

BLUE 2200 nm
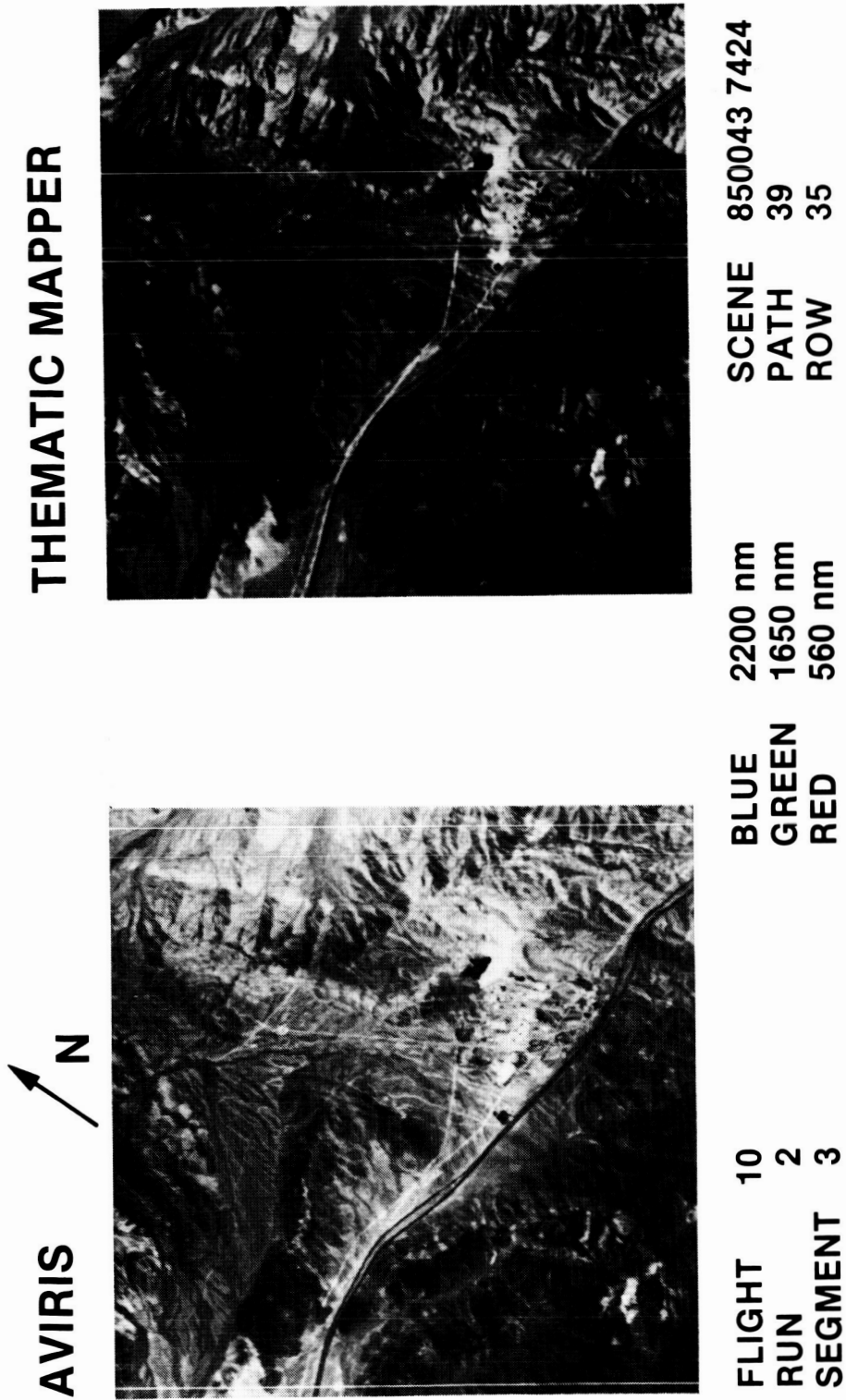GREEN 1650 nm
RED 560 nm

FLIGHT 10
RUN 2
SEGMENT 3

Figure 14. Comparison of AVIRIS and Thematic Mapper images of Mountain Pass, CA, at equivalent spectral wavelengths and bandwidths. AVIRIS more completely resolves the two strands of Interstate 15 as well as the fine stratigraphic units and drainage patterns found at the test site (refer to slide No. 12).

4.4 Signal-to-Noise Performance.

An in-flight assessment of the noise performance was developed through calculation of the standard deviation of each AVIRIS channel from data acquired over a nearly homogeneous region of the Ivanpah Playa. This analysis relates signal variation over a spatially homogeneous region to in-flight instrumental noise. An independent assessment of noise is found through determining the statistical variation in the dark current measured at the end of each image line. Results from each of these analyses are plotted in Figure 15. In each spectrometer, the variation calculated in the instrument response over the playa is similar in magnitude to the variation in the end-of-line dark current, establishing the dark current statistics as a valid estimator of instrument noise. Accurate determination of noise based solely on the dark current demonstrates AVIRIS noise for these data is independent of the radiance incident at the instrument. These results are consistent with laboratory measurements dark current and integrating sphere signal levels and statistics (Chrien, 1988).
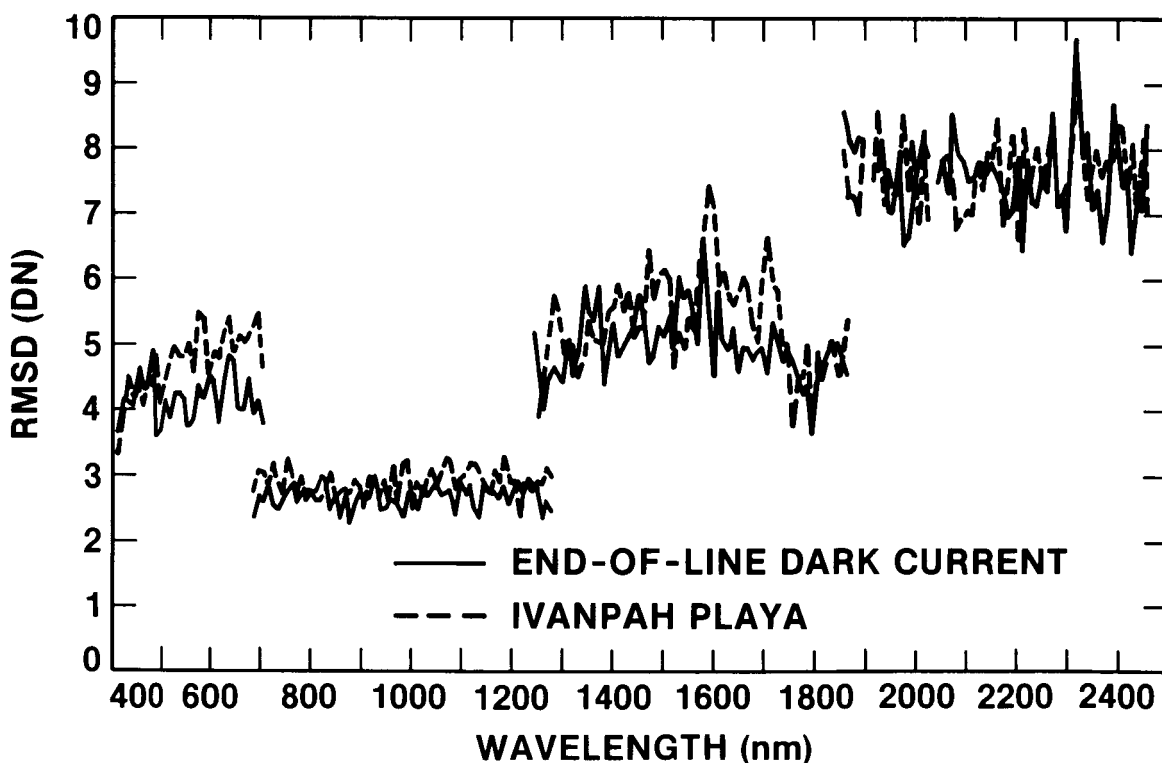

Figure 15. Standard deviation of AVIRIS end-of-line dark current and image data over a homogeneous section of Ivanpah Playa. The statistical variation of the dark current accounts for the variation observed in the data over the playa, demonstrating dark current statistics to be a good estimator of instrument noise.

Determination of in-flight noise without requiring a large homogeneous surface target provides an approach for calculating the signal-to-noise ratio for any region of interest in the AVIRIS data. The ratio of average instrument response, with dark current subtracted, to the standard deviation of the dark current provides a valid estimate.

Because the signal incident at AVIRIS is determined by the solar illumination, surface reflectance, atmospheric attenuation and atmospheric scattering, the directly calculated signal-to-noise is not comparable to determinations under other conditions or in the laboratory. This issue is resolved by scaling the actual instrument response to the AVIRIS reference radiance prior to calculating the signal-to-noise. The reference radiance is constrained by the conditions given in Table 4. A comparison of the AVIRIS reference radiance model and Ivanpah Playa radiance calculated is shown in Figure 16. The Ivanpah radiance values were calculated using LOWTRAN 7 and the PIDAS and atmospheric optical depth data as previously described.

TABLE 4.

Parameters defining the AVIRIS reference radiance.

Radiative Transfer Code	LOWTRAN 7
Atmospheric model	Midlatitude summer
Atmospheric aerosols	Rural 23 km visibility
Observer altitude	0 km
Target altitude	0 km
Target reflectance	0.50
Date	Summer solstice
Hour	Solar noon
Latitude	45 degrees
Radiance used	Reflected component

A signal-to-noise ratio was calculated by forming a ratio of image signal level over Ivanpah Playa, after dark current subtraction, to image noise values derived from end-of-line dark current statistics. To compare the in-flight signal-to-noise ratio for Ivanpah Playa to laboratory and other in-flight determined values, an AVIRIS reference radiance model was used to normalize the Ivanpah signal levels. Both the normalized signal levels and the observed signal levels were then divided by the observed noise to produce the signal-to-noise plots shown in Figure 17. In terms of the reference radiance model, spectrometer A had a peak signal-to-noise ratio of 90 - 100 to 1, B of 60 to 1, C of 40 - 50 to 1, and D of about 20 to 1 on July 30, 1987.
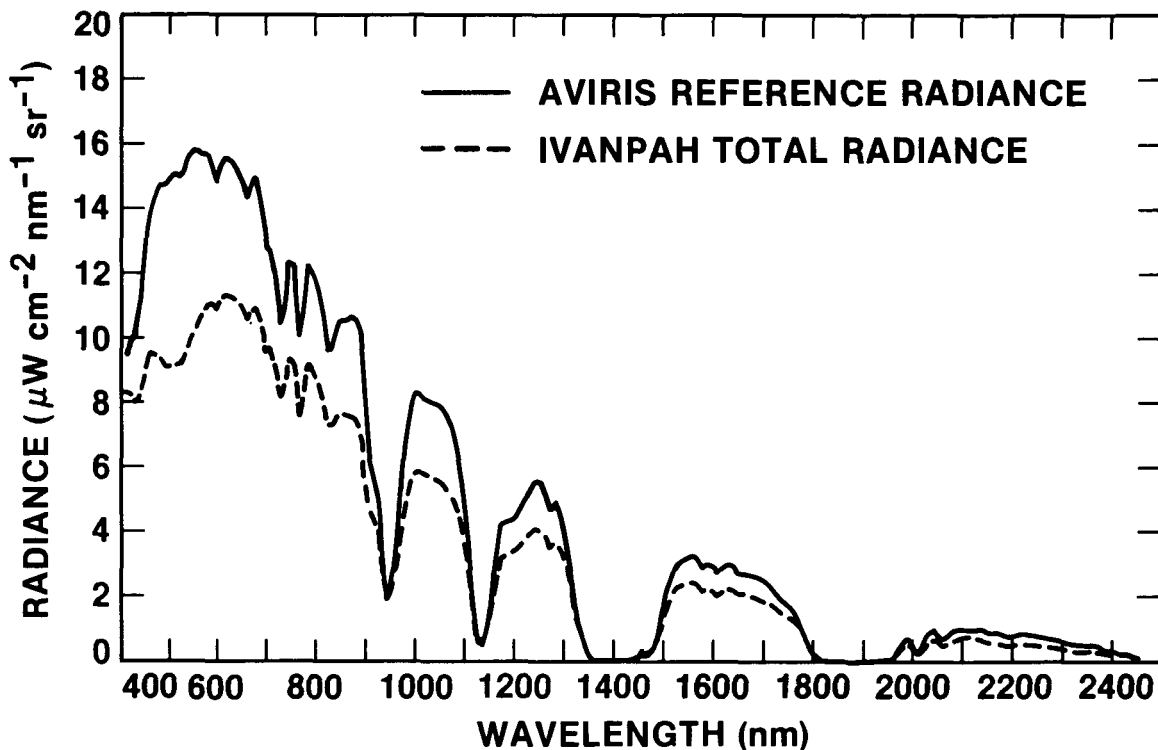

Figure 16. A plot of the AVIRIS reference radiance used to scale actual radiance falling on the instrument for intercomparison of signal-to-noise performance between data sets acquired in flight or in the laboratory.
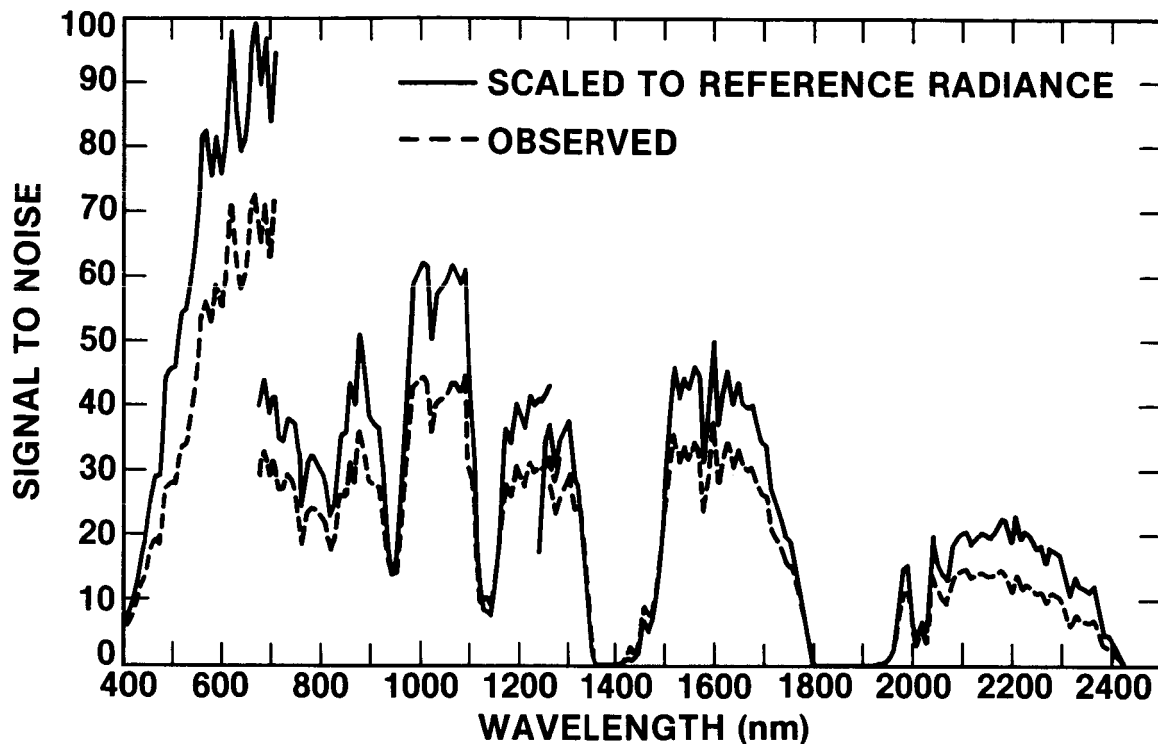
Figure 17. AVIRIS observed signal-to-noise performance over Ivanpah Playa calculated by a ratio of mean signal over the playa to standard deviation of the corresponding end-of-line dark current, and signal-to-noise scaled to the AVIRIS reference radiance. The scaled signal-to-noise can be compared to any other similarly scaled AVIRIS data set to assess stability of the radiometric response function of the instrument.

5.0 CONCLUSION

Through the evaluation of the in-flight performance and application of in-flight spectral and radiometric calibrations to the AVIRIS data acquired on July 30, 1987, a number of conclusions are reached. (1) AVIRIS successfully resolves narrow spectral absorption features both on the surface and in the atmosphere. (2) The empirical line algorithm compensates for both additive and multiplicative factors and directly transforms in-flight instrument response to reflectance. (3) Based on both surface and atmospheric absorption features, a shift of several nanometers in spectral position relative to the pre-flight season calibration is shown in spectrometers B and D. (4) Comparison of the modeled atmospheric radiance and the calibrated AVIRIS radiance show a degradation in spectral response function in spectrometers A and B. (5) A least squares residual algorithm minimizing on the LOWTRAN 7 and the pre-season calibrated AVIRIS radiance for both spectral position and

response function generates an improved spectral calibration. (6) In-flight modeled radiance based on concurrent in situ surface and atmospheric measurements predicts higher radiance in spectrometers A and B, with lower radiance in C and D relative to the pre-flight season laboratory calibration, thus demonstrating a corresponding change in radiometric response functions. (7) The modeled radiance provides a direct approach to in-flight radiometric calibration. (8) Comparison of coincident Thematic Mapper and AVIRIS imagery shows AVIRIS is resolving finer surface detail and shows good spatial geometry. (9) Variation in the end-of-line dark current is a valid estimate of noise in the AVIRIS data.

Thus, assessment of the spectral, radiometric, spatial and signal-to-noise properties of AVIRIS can be achieved with a combination of in situ surface and atmospheric measurements in conjunction with a suitable radiative transfer code, providing a tool for sensor in-flight performance evaluation and calibration.

6.0 ACKNOWLEDGEMENTS

7.0 REFERENCES

Adams, J. W., "The visible region absorption spectra of rare-earth minerals," The Amer. Min. 50, 356-367, (1965)

Chrien, T. G., personal communication, (1988).

Conel, J. E., R. O. Green, V. Carrere, J. S. Margolis, R. E. Alley, G. Vane, C. J. Bruegge and B. L. Gary, "Mapping atmospheric water vapor with the Airborne Visible/Infrared Imaging Spectrometer (AVIRIS) at Mountain Pass, California," in proceedings of the Airborne Visible/Infrared Imaging Spectrometer (AVIRIS) Performance Evaluation Workshop, G. Vane, Ed., JPL Publication 88-38, pp TBD (1988a).

Conel, J. E., R. O. Green, R. E. Alley, C. J. Bruegge, V. Carrere, J. S. Margolis, G. Vane, T. G. Chrien, P. N. Slater, S. F. Biggar, P. M. Teillet, R. D. Jackson, M. S. Moran, "In-flight radiometric calibration of the Airborne Visible/Infrared Imaging Spectrometer (AVIRIS)," in Proceedings SPIE Conference on Recent Advances on Sensors, Radiometry and Data Processing for Remote Sensing, 924, 168-178, (1988b).

Conel, J. E., R. O. Green, G. Vane, C. J. Bruegge and R. E. Alley, "AIS-2 radiometry and a comparison of methods for the recovery of ground reflectance," in Proceedings of the Third Airborne Imaging Spectrometer Data Analysis Workshop, G. Vane, Ed., JPL Publication 87-30, 18-47 (1987).

Goetz, A. F. H., "The Portable Instant Display Analysis Spectrometer (PIDAS)," in Proceedings of the Third Airborne Imaging Spectrometer Data Analysis Workshop, (ed Vane, G.) JPL Publication 87-30, 8-17 (1987).

Herman, B., A. J. LaRocca and R. E. Turner, "Atmospheric Scattering," in The Infrared Handbook (eds W. L. Wolfe and G. J. Zissis) 4-1-76, Environmental Research Institute of Michigan, (1978).

Kneizys, F. X., E. P. Shettle, G. P. Anderson, L. W. Abrew, J. H. Chetwynd, J. E. A. Shelby, S. A. Clough, and W. O. Galery, "Atmospheric Transmittance/Radiance: computer code LOWTRAN 7," (in press) (1988).

Macenka, S. A. , and M. P. Chrisp, "Airborne Visible/Infrared Imaging Spectrometer (AVIRIS) spectrometer design and performance," in Imaging Spectroscopy II, SPIE 834, 32-49, (1987).

Olson, J. C., D. R. Shawe, L. C. Pray, and W. N. Sharp, "Rare-Earth mineral deposits of the Mountain Pass district San Bernardino county California," Geological Survey Professional Paper 261, 75 (1954).

Porter, W. M., H. T. Enmark, "A system overview of the Airborne Visible/Imaging Spectrometer (AVIRIS)," Proceedings SPIE Conference on Imaging Spectroscopy II (San Diego, CA, 20-21 August, 1987), 834, 22-31 (1987).

Shaw, G. E., J. A. Reagan and B. H. Herman, "Investigation of atmospheric extinction using direct solar radiation measurements made with a multiple wavelength radiometer," J. Appl. Meteorol., 12, 374-380, (1973).

Vane, G., T. G. Chrien, E. A. Miller, J. H. Reimer, "Spectral and radiometric calibration of the Airborne Visible/Infrared Imaging Spectrometer (AVIRIS)," Proc. SPIE Conference on Imaging Spectroscopy II (San Diego, CA, 20-21 August, 1987), 834, 91-106 (1987).

Vane, G., T.G. Chrien, J.H. Reimer, R.O. Green, J.E. Conel, "Comparison on laboratory calibrations of the Airborne Visible/Infrared Imaging Spectrometer and the beginning and end of the first flight season," Proc. SPIE Conference on Recent Advances on Sensors, Radiometry and Data Processing for Remote Sensing, 924, 168-178, (1988).